**University of Bath**

**Alternative formats**
If you require this document in an alternative format, please contact:
openaccess@bath.ac.uk

# Tin(II) Ureide Complexes: Synthesis, Structural Chemistry and Evaluation as SnO precursors.

Thomas Wildsmith,[a,b] James D. Parish,[a] Ibbi Y. Ahmet,[a,b] Kieran C. Molloy,[a] Michael S. Hill[a] and Andrew L. Johnson.[a]*

a: Department of Chemistry, University of Bath, Claverton Down, Bath BA2 7AY, United Kingdom.

b: Centre for Sustainable Chemical Technologies, University of Bath, Bath BA2 7AY, United Kingdom.

## Abstract

In an attempt to tailor precursors for application in the deposition of phase pure SnO we have evaluated a series of tin (**1**–**6**) ureide complexes. The complexes were successfully synthesised by employing N,N'-trialkyl-functionalised ureide ligands, in which features such as stability, volatility, and decomposition could be modified with variation of the substituents on the ureide ligand in an attempt to find the complex with the ideal electronic, steric or coordinative properties which determine the fate of the final products. All the complexes were characterized by NMR spectroscopy as well as elemental and where applicable thermogravimetric (TG) analysis. The single-crystal X-ray diffraction studies of **2**, **3**, **4** and **6** revealed that the complexes crystalise in the monoclinic space group *P2(1)/n* (**2** and **4**) or in the triclinic space group *P-1* (**3** and **6**) as monomers. Reaction with phenyl isocyanate results in the formation of the bimetallic species **5**, which crystalises in the triclinic space group *P-1*, resulting in incomplete insertion into the Sn-NMe$_2$ bonds verses mesityl-isocyanate which produces a monomeric double insertion product, **6**, under the same conditions, indicating a difference in reactivity between phenyl-isocyanate and mesityl-isocyanate with respect to insertion into Sn-NMe$_2$ bonds. The metal centres in these complexes are all four-coordinate, displaying either distorted trigonal bipyramidal or trigonal-bipyramidal geometries. The steric influence of the imido-ligand substituent has a clear effect on the coordination mode of the ureide ligands, with complexes **2** and **6**, which contain the cyclohexyl and mesityl ligands, displaying $\kappa^2$-O,N coordination modes, whereas $\kappa^2$-N,N' coordination modes are observed for the sterically bulkier t-butyl and adamantyl derivatives, **3** and **4**. The thermogravimetric analysis of the complexes **3** and **4** exhibited excellent physicochemical properties with clean single-step curves and low residual masses in their TG analyses suggesting there potential utility of these systems as MOCVD and ALD precursors.

## Introduction

The combination of visible range transmittance and electrical conductivity designate enormous potential to transparent conducting and semiconducting oxides for the development of transparent electronic devices.[1, 2] Although a wide variety of photovoltaic, electrochromic and display applications may be envisaged from the implementation of transparent complementary metal oxide semiconductor (CMOS) devices, the prospects for success are at present severely limited by the dearth of suitable *p*-type oxide materials.[3-5] As a result, the discovery of *p*-type charge transport in stannous oxide, SnO,[6-10] has prompted increasing attention to its fabrication, in particular as a thin film. While a variety of physical vapour deposition routes to SnO thin films have been evaluated,[8, 11-13] chemical routes, including atomic layer and chemical vapour deposition from reactive metalorganic precursors, are restricted to a handful of examples (Figure 1). This paucity of precursors stems, in part, from a requirement for stringent control of the Sn(II) oxidation state in both the precursor and the final SnO thin films.[14] In an attempt to address this limitation we have initiated a study of stannous complexes which act as single source molecular precursors for the deposition of SnO thin films. We have previously reported that use of [Sn(OSiMe$_3$)$_2$]$_2$ (Fig.1A) (aerosol-assisted CVD),[15] [Sn$_6$(O)$_4$(OSiMe$_3$)$_4$] (Fig.1B) (liquid-injection CVD)[15] and a variety of homoleptic stannous alkoxides (Fig.1C) (AACVD) provide viable precursors to SnO through the maintenance of the Sn(II) oxidation state.[16] Most successfully, we have also provided a preliminary account of an easily synthesised Sn(II) bis(ureide), [Sn{N(Bu$^t$)C(O)NMe$_2$}$_2$] (Fig.1D), which may be utilised as a single source precursor for the aerosol-assisted CVD of phase pure SnO at temperatures as low as 250°C.[17] To-date only three precursors capable of depositing phase pure SnO using atomic layer deposition (ALD), i.e. [Sn{OCMe$_2$CH$_2$NMe$_2$}$_2$][18] (Fig.1E), [Sn{OC($^t$Bu)=NOEt}$_2$][19, 20] (Fig.1F) and [Sn{N($^t$Bu)CMe$_2$CH$_2$N($^t$Bu)}$_2$][21] (Fig.1G) have been realised.
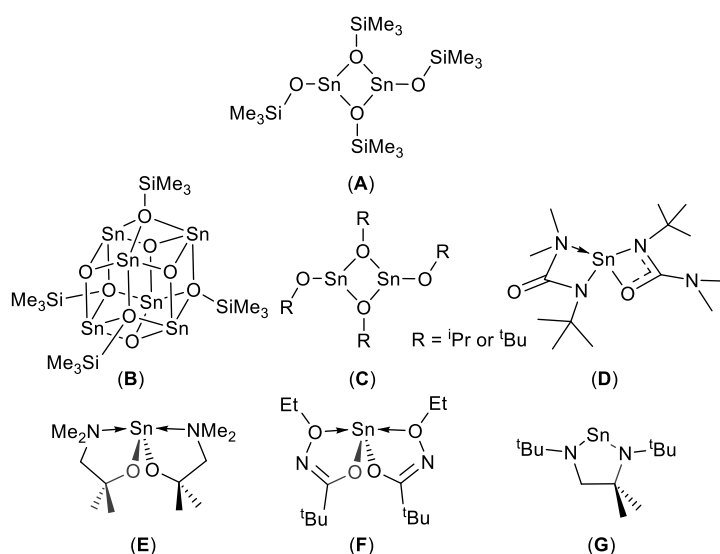


**Figure 1:** Molecular Precursors used for the CVD (A-D) or ALD (E-G) SnO thin films.

Monoanionic ureide ligands of the general form shown in Figure 2 have a range of possible coordination behaviors, from $\kappa^2$-chelating (**I**,[17, 22, 23] **II**[24] and **III**[17, 24, 25]) or bridging $\mu^2$-$\kappa$-N,O (**IV**)[26-28] and $\mu$-$\eta^1$:$\eta^2$ (**VII**),[29] to face capping-chelating $\mu^3$-$\eta^2$ (**VIII**) modes,[30] offering a greater structural diversity when coordinated to main group, transition metal and f-block elements, than the related carboxylate, amidinate or guanidinate ligands, all of which have been more extensively studied than ureide ligands. To the best of our knowledge, potential bridging $\mu^2$-$\kappa$-N,N' modes **V** and **VI** have yet to be observed.
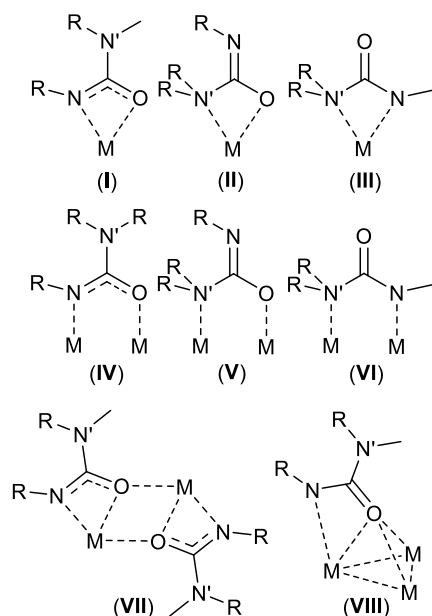


**Figure 2**: Possible coordination modes of monoanionic ureide ligands.

We have previously demonstrated that both ureides and thio-ureides have a rich chemistry, with their respective metal complexes capable of acting as single source precursors for the phase controlled deposition, of Cu,[31] SnO,[17] SnS[32] and ZnS.[33] In the present work, we describe a range of homo- and heteroleptic tin(II)-ureide complexes, which have been synthesized by direct reaction of the aryl- and alkyl-isocyanates with [Sn{NMe$_2$}$_2$]$_2$, in an attempt to fine tune their electronic, steric or coordinative properties, which determine the fate of the final products, for a given ligand set. We also report investigations into the thermal stabilities of these complexes.

**Results and Discussion**

The tin(II) ureide complexes **1**–**6** were synthesised by the reaction of [Sn{NMe$_2$}$_2$]$_2$ and the appropriate alkyl (**1**–**4**) or aryl (**5**–**6**) isocyanate in toluene (Scheme 1). Compounds **2**–**6** were isolated as colourless solids in near quantitative yields, while **1** was an orange/brown oil which was prone to decomposition and could be characterised only by NMR spectroscopy.
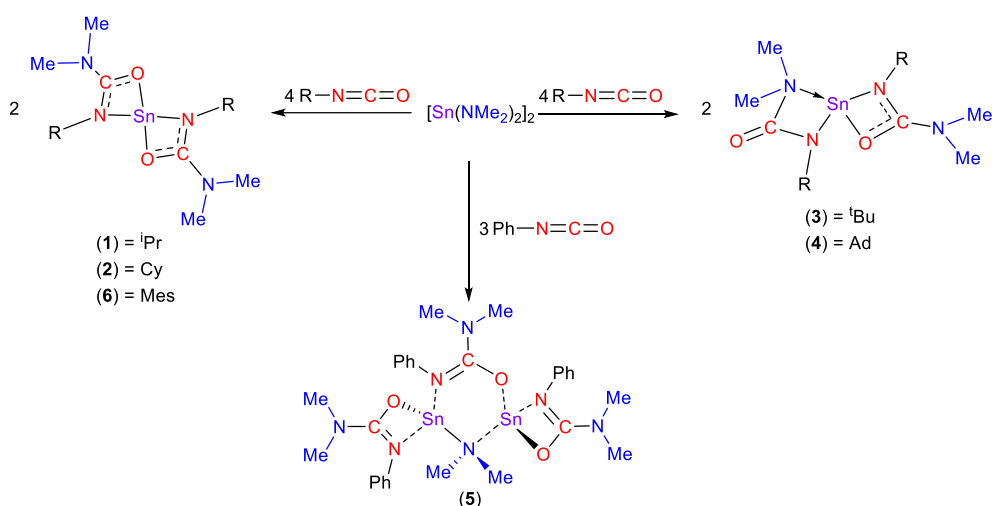
**Scheme 1**: Synthesis of the Sn(II) ureide complexes **1-6**, via the insertion of isocyanates into Sn-NMe$_2$ bonds.

Attempts to isolate compound **1** were unsuccessful. Removal of the reaction solvent yielded an orange-brown oil, the NMR spectra of which evidenced the presence of two different environments for each of the isopropyl and dimethylamide groups. All attempts to crystallise the compound proved unsuccessful. The formation of the ureide, however, was confirmed by performance of the reaction in d$_8$-toluene and monitoring of the solution by multinuclear NMR spectroscopy. The $^1$H NMR spectrum for **1** comprised resonances at δ 1.24 and 3.95 ppm corresponding to the methyl and methine protons of the {N-$^i$Pr} group and a further resonance at δ 2.57 ppm. which was assigned to the {NMe$_2$} unit. The $^{13}$C{$^1$H} NMR spectrum was also consistent with a homoleptic formulation, displaying resonances at δ 25.3, 39.0 and 47.2 ppm assigned to the {N-$^i$Pr} methyl and methine and {NMe$_2$} carbon nuclei respectively. A resonance at δ 167.2 ppm could also be assigned to the N$C$(N)O backbone carbon. The $^{119}$Sn{$^1$H} NMR spectrum comprised of a single resonance at δ −307 ppm, at considerably lower ppm than the starting amide, [Sn{NMe$_2$}$_2$: δ = +125 ppm].

Reaction of the alkyl isocyanates (cyclohexyl isocyanate, tert-butyl isocyanate and adamantyl isocyanate) proceeded similarly to form complexes **2-4** respectively. The $^1$H NMR spectra for the complexes **2-4** are again unexceptional and contained all the anticipated resonances in the appropriate ratios. As with the isopropyl derivative (**1**) a single resonance in the $^{13}$C{$^1$H} NMR spectra of **2-4** at *ca.* δ = 166-167 ppm could be assigned to the central carbon of the N-$C$(N)-O backbone of the ureide ligands. The $^{119}$Sn{$^1$H} NMR spectra for **2-4** each displayed a single resonance at δ = −310 (**2**), −357 (**3**) and −351 (**4**) ppm, respectively.

The $^1$H NMR spectra of complexes **3** and **4** at room temperature display two sets of resonances associated with the {$^t$Bu} and {NMe$_2$} moieties of the ureide ligands in **3** (a 9:6 ratio by integration at δ 1.45 and 2.44 ppm)[17] and the {Ad} and {NMe$_2$} moieties of the ureide ligands in **4** (a 6:3:6:6 ratio by integration). Prompted by our observations in the solid state (vide infra), that complexes **3** and **4** display

an aniso-bidenticity of the ureide ligands, such that $\kappa^2$-*N,O* and one $\kappa^2$-*N,N′* bonding modes are observed, variable temperature NMR studies were undertaken. In the case of complex **3**, variable temperature $^1$H NMR studies (298 K -208 K), in $d_8$-toluene, evidenced a clear splitting of the singlet resonance at $\delta$ =1.45 ppm (298 K) into two resonances at d =1.25 and 1.59 ppm respectively, with a maximum peak to peak separation ($\Delta\nu$) of 142 Hz at 208 K (Figure 3). We believe these two resonances to be associated with the aniso-bidentate form of 3, observed in the solid state. Warming to higher temperatures, i.e. >234 K, coalesce of these two signals in the $^1$H NMR spectrum is observed, consistent with an *in-solutio* intramolecular rearrangement of the $\kappa^2$-*N,O* and $\kappa^2$-*N,N′* bonding modes, to a averaged iso-bidentate ($\kappa^2$-*N,O*) structure as shown in Figure 3. However, it should be noted that it is highly unlikely that the single resonance at $\delta$ = 145 ppm observed in the $^1$H NMR spectrum at 298K can be attributed to the *bis*-$\kappa^2$-*N,O* isomer of complex **3**. Rather, we would suggest that ligand rearrangement is sufficiently fast at temperatures >258 K, to show an averaged signal for the {tBu} groups in the $^1$H NMR spectra. While we are unable to comment on the precise nature of the ligand rearrangement process it seems reasonable to assume that a low-energy bond-breaking mechanism, with a calculated $\Delta G^{\ddagger}$ for the rearrangement process of $\Delta G^{\ddagger}$ = +46 kJ mol$^{-1}$, is most likely, as similar processes have been observed elsewhere.[34]
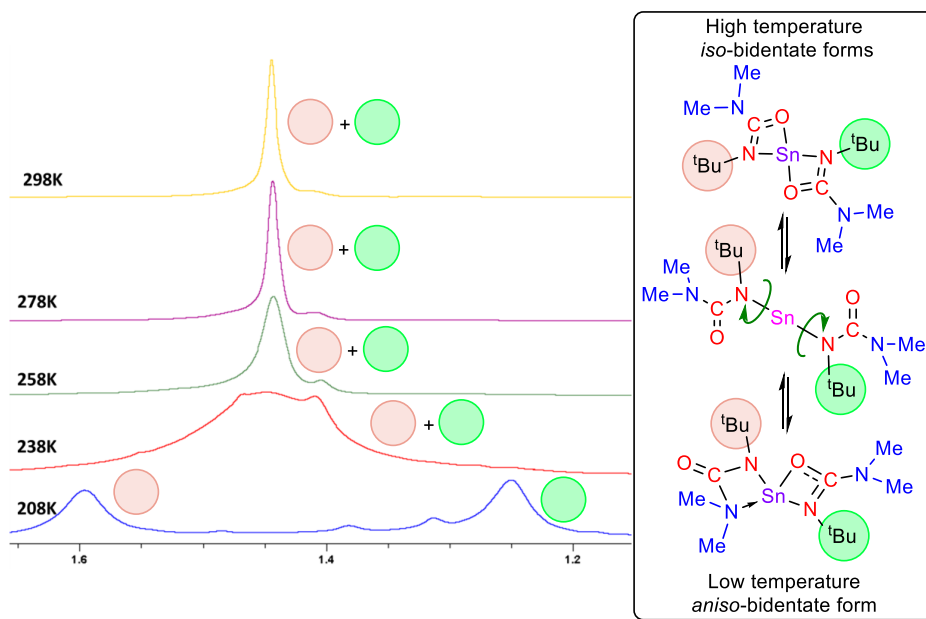


**Figure 3**: Variable temperature 298K to 208K (+25 °C to –65 °C) $^1$H NMR spectra (500 MHz, $d_8$-toluene) for compound **3**, focusing on the *tert*-butyl resonance. The hypothesised dynamic process occurring in solution in 3 (right): At low temperatures (< 238K) the fluxional process of ligand interchange is slow, resulting in two {$^t$Bu} resonances in the $^1$H NMR spectrum of **3**. At higher temperatures (> 258K) the fluxional process fast resulting in an averaged signal, such that one {$^t$Bu} resonance is observed in the $^1$H NMR spectrum.

In the case of the adamantyl derivative, **4**, meaningful interpretations of VT NMR data could not be obtained due to the overlapping resonances of the {NMe$_2$} moieties and the various {CH} and {CH$_2$} resonances associated with the adamantyl group.

Contrastingly, the reaction of two equivalents of phenyl isocyanate with [Sn{NMe$_2$}$_2$]$_2$ resulted in the isolation of a material, which, when analysed by NMR spectroscopy, presented a more complex system (**5**). The $^1$H NMR spectrum (296 K) consisted of one broad singlet peak at δ = 2.27 ppm (18H *i.e.* 3x{NMe$_2$}) and a broad resonance at δ = 2.76 ppm {NMe$_2$}. The $^1$H NMR spectra also contained three distinct broad multiplet resonances between δ = 6.75 – 7.14 ppm (in a 3H:6H:6H ratio) associated with three {Ph} groups. VT $^1$H NMR of **5** (323 K) clearly shows coalescence of the signals into one set of ureide resonances and one {NMe$_2$} resonance. However, thermal instability of the complex at elevated temperatures precluded exhaustive multinuclear NMR studies. The $^{13}$C{$^1$H} NMR (296 K) spectrum consisted of resonances, one sharp and one broad, at δ = 38.2 and 40.0 ppm, suggestive of two discrete {NMe$_2$} environments. At lower-field, resonances at δ = 121.8, 124.4, 128.9 and 147.3 ppm are associated with the *para*, *ortho*, *meta*, and *ipso* carbons of the phenyl groups respectively. A further peak in the spectrum at δ = 164.8 ppm is assigned to the central carbon of the N-*C*(N)-O backbone of the ureide ligands. The $^{119}$Sn{$^1$H} NMR spectrum displayed a broad resonance at δ −217, at significantly lower field than observed for complexes **1**-**4**.

These data are consistent with the formation of the unsymmetrical bimetallic complex, **5**, observed in the solid state (vide infra), as shown in Scheme 1. Isocyanate insertion into three of the four Sn-NMe$_2$ bonds of [Sn{NMe$_2$}$_2$]$_2$ produces two different {NMe$_2$} environments, *i.e.* three ureide {OC(NMe$_2$)NPh} ligands, and one bridging {NMe$_2$}, which in solution undergo rapid exchange such that all three ureide ligands are equivalent, as indicated by the single resonance in the $^{13}$C{$^1$H} NMR spectra associated with the central carbon of the N-*C*(N)-O backbone. Elemental analysis is also consistent with the formation of a bimetallic complex of the formula [{PhNC(O)NMe$_2$}$_3$Sn$_2${NMe$_2$}] (Scheme 1).

Despite repeated attempts to identify and isolate the desired *bis*-ureide product, [{PhNC(O)NMe$_2$}$_2$Sn], by varying the ratio of isocyanate to tin(II) amide, as well as reaction conditions, we have been to-date, unsuccessful in our attempts. Similarly, attempts to prepare and isolate the mono-insertion product [{PhNC(O)NMe$_2$}Sn{NMe$_2$}] were unsuccessful, often resulting in the isolation of complex **5**. Prompted by our observations in the solid state, variable temperature $^1$H NMR studies of complex **5**, in d$^8$-THF, were undertaken. Reduced temperature $^1$H NMR studies (238 K) evidenced a clear splitting of the three broad multiplet resonances between δ = 6.75 – 7.14 ppm observed at room temperature into two sets of multiplets between 6.70-7.00 (10H) and 7.02-7.25 (5H), suggestive of a "freezing out" of fluxionality in the ureide ligands and resolution into two distinct sets of resonances. A similar splitting

effect is observed in the {NMe$_2$} region of the spectra (2.16-2.78 ppm), however meaningful interpretations here are limited by the overlapping resonances of the bridging {NMe$_2$} unit.

Reaction of mesityl-isocyanate with [Sn{NMe$_2$}$_2$] in a 2:1 ratio resulted in the isolation of a material, which when analysed by NMR spectroscopy displays four sets of resonances associated with the {Mes} and {NMe$_2$} moieties in ratios of 3H:6H:6H:2H by integration at δ = 2.17 (*p*-Me), 2.35 (*o*-<u>Me</u>), 2.37 (NMe$_2$) and 6.75 (CH) ppm, respectively. A resonance in the $^{13}$C{$^1$H} NMR spectra of **6** at δ = 164.4 ppm could be assigned to the central carbon of the N-*C*(N)-O backbone of the ureide ligands. The $^{119}$Sn{$^1$H} NMR spectra for **6** displayed a single resonance at δ = −353 ppm comparable to the *bis*-ureide complexes **1**-**4**, rather than the bimetallic *tris*-ureide complex **5**.

The $^{119}$Sn{$^1$H} NMR chemical shifts for the five compounds **1**-**4** and **6** (table 1) correlate well with shifts previously reported for homoleptic tin(II) *bis*-amidinates (δ −255 to −397 ppm) and *bis*-guanidinates (δ = −377 to −432 ppm), all of which have been identified as containing unambiguously four-coordinate Sn(II) centres in solution and may be interpreted to indicate a similar level of charge donation irrespective of the donor atoms of the two bidentate ligands. The resonances are, however, significantly downfield of the only other reported Sn(II) *iso*-ureide complex; the related homoleptic κ$^2$-*N,N*-bound *iso*-ureide species, Sn[N(R)C(OSiMe$_3$)NR]$_2$ [R = 3,5-(CF$_3$)$_2$C$_6$H$_3$], which was reported to occur at δ = −557ppm.[35]


**Molecular structures of tin(II) ureide complexes**

The solid-state structures of complexes **2**–**6** were confirmed by single-crystal X-ray diffraction analysis. While we have previously described the molecular structure of **3**,[17] it is included here for comparative purposes.

The molecular structures of the cyclohexyl and mesityl derivatives, **2** and **6**, which have much in common, are shown in Figure 4; a summary of selected bond lengths and angles can be found in Table 1.
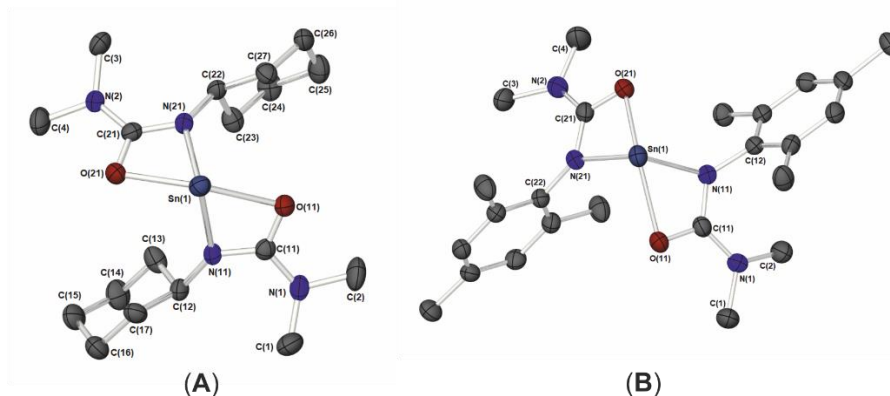
**Figure 4:** Molecular structures of the *bis*-ureide complexes **2** (**A**) and **6** (**B**). Thermal ellipsoids are shown at 50% probability. Hydrogen atoms have been omitted for clarity.

**Table 1.** Selected bond lengths (Å) and angles (°) for complex **2** and **6**.

| | Bond lengths (Å) | | | Bond Angles (°) | |
|---|---|---|---|---|---|
| | **2** | **6** | | **2** | **6** |
| Sn(1)-O(11) | 2.364(2) | 2.3374(17) | O(11)-Sn(1)-O(21) | 135.10(7) | 125.19(6) |
| Sn(1)-O(21) | 2.295(2) | 2.2763(16) | N(11)-Sn(1)-N(21) | 100.46(10) | 100.62(7) |
| Sn(1)-N(11) | 2.186(3) | 2.2209(19) | O(11)-Sn(1)-N(21) | 93.08(8) | 87.07(7) |
| Sn(1)-N(21) | 2.176(2) | 2.1985(18) | O(21)-Sn(1)-N(11) | 90.89(8) | 85.46(6) |
| O(11)-C(11) | 1.280(4) | 1.284(3) | | | |
| C(11)-N(11) | 1.328(4) | 1.338(3) | O(11)-Sn(1)-N(11) | 57.93(8) | 57.96(6) |
| C(11)-N(1) | 1.369(4) | 1.358(3) | O(21)-Sn(1)-N(21) | 59.04(8) | 59.02(6) |
| O(21)-C(21) | 1.290(4) | 1.289(3) | | | |
| C(21)-N(21) | 1.326(4) | 1.331(3) | O(11)-C(11)-N(11) | 115.7(3) | 114.9(2) |
| C(21)-N(2) | 1.369(4) | 1.353(3) | O(21)-C(21)-N(21) | 114.9(3) | 114.6(2) |

Complexes **2** and **6** both crystallise in the monoclinic (*P2₁/n*) and triclinic (*P-1*) space group with one molecule per asymmetric unit cell.

Both complexes were found to exist as monomeric species with the tin(II) centres possessing a four-coordinate geometry, heavily influenced by the stereochemically active lone pair at the tin(II) centre. In each case the tin coordination environments can be ascribed as distorted trigonal bipyramidal and distorted square based pyramidal geometries respectively, as determined by the geometric index parameter $\tau$ (**2**: $\tau = 0.58$ **6**: $\tau = 0.41$)[36, 37] with the stereochemically active lone pairs situated in the equatorial and apical positions, respectively.

Both complexes contain two ureide ligands coordinated to the tin(II) centres in a $\kappa^2$-*N, O* binding motif in which the nitrogen coordination is provided by the amido {N-R} donor rather than the amino {NMe₂} group. The ligands are positioned in a *transoid* configuration such that the bulkier cyclohexyl or mesityl groups are located on opposite sides of the molecule. This *transoid* configuration is expected due to the

bulky nature of the ligand, with this configuration being less sterically congested than any alternative *cisoid* orientation.

In both species the Sn–$O_{ureide}$ bonds [**2**: av 2.329 Å; **6**: av 2.306(2) Å] are slightly longer than the associated Sn–$N_{ureide}$ contacts [**2**: av 2.186(2) Å; **6**: av 2.205(2) Å]. The accompanying N-C and C-O bond lengths [C-N(R): av 1.327 Å (**2**), av 1.335 Å (**6**); C-NMe$_2$: av 1.368 Å (**2**), av 1.356 Å (**6**); C-O: av 1.285 Å (**2**), av 1.286 Å (**6**)] are in the range associated with partial double bonds. An examination of the bond angles and bond lengths of the ureide ligands indicate that the π electrons of the ureato fragments are delocalized in the NC(N)O core.

We previously described, in preliminary form, the solid-state structure for compound **3,** which crystallises in the triclinic space group *P-1*. Its structure is shown in Figure 3, and the bond lengths and angles listed in Table 2 are provided here for purposes of comparison and clarity of presentation. Figure 5 also shows the solid-state molecular structure of the adamantyl derivative **4**, which crystallises in the monoclinic space group *P2$_1$/n*. Selected bond lengths and angles are listed in Table 2. alongside those of **3**.

As can clearly be seen in Figure 5, complexes **3** and **4** possess very different solid-state molecular structures to complexes **2** and **6**. While all four complexes contain four coordinate Sn(II) centres, similarities are limited. In contrast to the κ$^2$-*N,O* bonding modes observed for the ureide ligands of compounds **2** and **6**, the solid-state structure of compounds **3** and **4** incorporates one κ$^2$-*N,O* and one κ$^2$-*N,N'* bound ureide with the two bulky tert-butyl and adamantyl groups, respectively, located with a *cisoid* relationship to each other with respect to the equatorial plane of the *pseudo* bipyramidal coordination geometry (**3**: τ = 0.63; **4**: τ = 0.59).[36, 37] Consequently, the majority of the ligands' bulk is located on the same side of the compound. This observation is consistent with the low temperature (−65 °C) solution state observation of two {$^t$Bu} environments in the $^1$H and $^{13}$C{$^1$H} NMR spectra of complex **3**, which interchange at elevated temperatures. This ability to exchange between the κ$^2$-*N,O* and κ$^2$-*N,N'* coordination modes in solution, and under conditions relevant to AACVD, may be pertinent to its application as a single source SnO precursor.
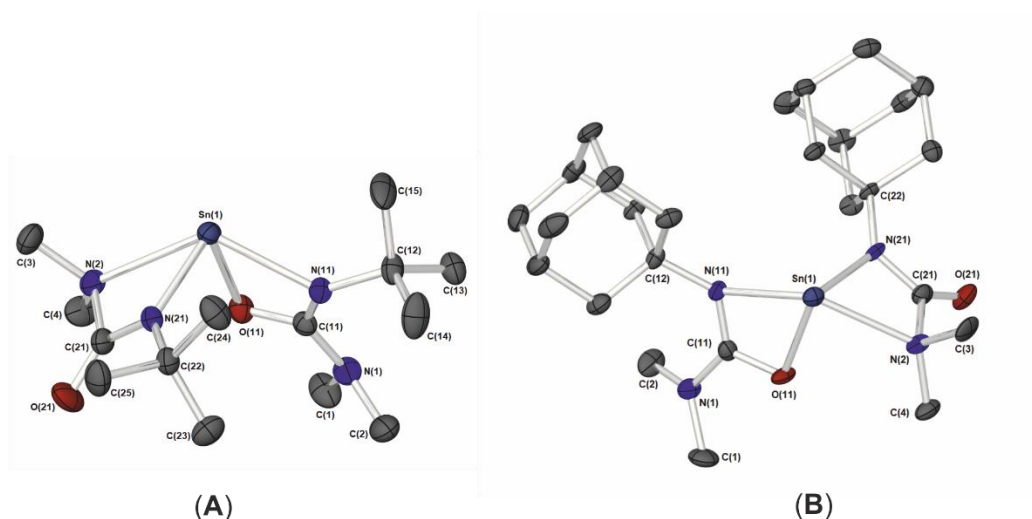
**Figure 5:** Molecular structures of (**A**) [Sn{N($^t$Butyl)C(O)NMe$_2$}$_2$][17] (**3**) and (**B**) [Sn{N(Adamantyl)C(O)NMe$_2$}$_2$] (**4**). Ellipsoids shown at 50% probability, hydrogen atoms omitted for clarity.

**Table 2.** Selected bond lengths (Å) and angles (°) for complexes **3** and **4**.

| Bond lengths (Å) | | | Bond Angles (°) | | |
|---|---|---|---|---|---|
| | **3**[17] | **4** | | **3**[17] | **4** |
| Sn(1)-O(11) | 2.1688(11) | 2.174(4) | N(11)-Sn(1)-O(11) | 59.15(4) | 58.93(16) |
| Sn(1)-N(11) | 2.3151(13) | 2.329(5) | N(21)-Sn(1)-N(2) | 57.90(5) | 58.36(17) |
| Sn(1)-N(2) | 2.4839(13) | 2.452(5) | N(11)-Sn(1)-N(2) | 127.90(4) | 129.32(16) |
| Sn(1)-N(21) | 2.1715(13) | 2.174(5) | O(11)-Sn(1)-N(21) | 90.11(5) | 94.02(17) |
| | | | | | |
| N(1)-C(11) | 1.369(2) | 1.380(8) | O(11)-C(11)-N(11) | 115.16(13) | 115.5(5) |
| N(11)-C(11) | 1.320 (2) | 1.317(7) | N(1)-C(11)-N(11) | 127.84(14) | 129.3(6) |
| O(11)-C(11) | 1.306(2) | 1.306(7) | N(1)-C(11)-O(11) | 115.16(13) | 115.5(5) |
| | | | O(21)-C(21)-N(21) | 131.57(16) | 132.9(6) |
| N(2)-C(21) | 1.482(2) | 1.507(8) | N(2)-C(21)-N(21) | 107.42(13) | 105.8(5) |
| N(21)-C(21) | 1.332(2) | 1.334(8) | N(2)-C(21)-O(21) | 121.00(14) | 121.2(6) |
| O(21)-C(21) | 1.220(2) | 1.209(7) | | | |

The Sn-O [**3**: 2.1688(11) Å; **4**: 2.174(4) Å] bond length of the $\kappa^2$-*N,O* bound ureide ligands are significantly shorter than those observed in **2** or **6** [**2**: av 2.329 Å; **6**: av 2.306 Å], a shortening compensated by elongation of the Sn(1)-N(11) bond [**3**: 2.3151(13) Å; **4**: 2.329(5) Å], *cf.* Sn-N bonds in **2** and **6** (*vide supra*). Furthermore, while the {NMe$_2$} unit of the $\kappa^2$-*N,O* bound ureide displays similar

characteristics to those seen in **1**, **2** and **4**, the degree of charge delocalisation, reflected in the dihedral angles {N(11)-C(11)-N(1)-C(2)} [(**3**): 45.4°; (**4**): 36.68°] and {O(11)-C(11)-N(1)-C(1)} respectively [(**3**): 11.8°; (**4**): 16.1°], are the lowest values observed in the series. For the $\kappa^2$-*N,N'* bound ureide ligands the Sn-N$_{imide}$ bonds [**3**: 2.1715(13) Å; **4**: 2.174(5) Å] are comparable to the Sn-N$_{imide}$ bonds found in **2** and **4**, while the Sn←NMe$_2$ bonds [**3**: 2.4839(13) Å; **4**: 2.452(5) Å] are the longest Sn-N interactions measured across the four compounds. As a consequence of this ligand bonding mode, the C-O bonds of the $\kappa^2$-*N,N'* bound ureide ligands are much shorter [**3**: 1.220(2) Å; **4**: 1.209(7)Å] than those observed in the $\kappa^2$-*N,O* ligands bound to the same metal [**3**: 1.306(2) Å; **4**: 1.306(7)Å], suggesting significant double bond character in the former of the two. Similar $\kappa^2$-*N,N'* bonding modes have been reported previously in handful of complexes.[38][24, 25, 39].
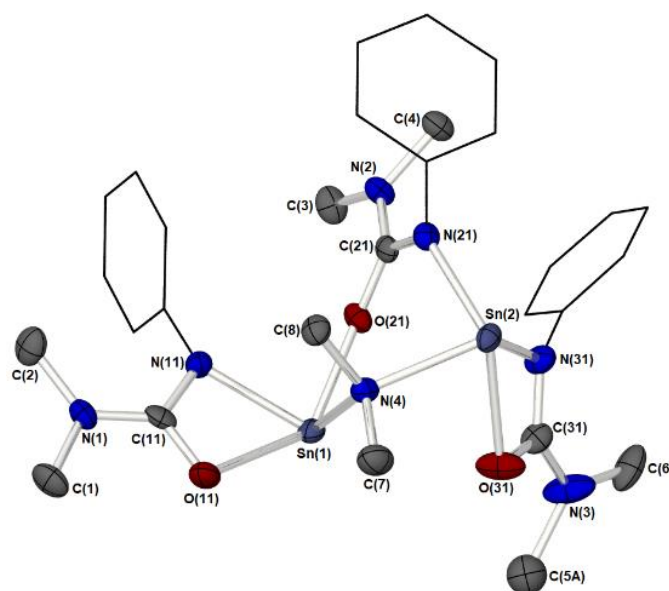


**Figure 6:** Molecular structure of [Sn$_2$\{$\mu$-NMe$_2$\}\{$\mu^2$-*N,O*-PhNC(NMe$_2$)O\}\{$\kappa^2$*N,O*-PhNC(NMe$_2$)O \}$_2$] (**5**). Ellipsoids shown at 50% probability, hydrogen atoms have been omitted for clarity. Phenyl-groups are shown as wire frames for clarity.

As noted above reaction of [Sn\{NMe$_2$\}$_2$]$_2$ with phenyl-isocyanate results in the formation of a bimetallic complex (**2**), which crystallises in the triclinic space group *P-1*, Figure 6. Selected bond lengths and angles for 5 are reported in Table 3. This unique molecular structure results from the insertion of three isocyanate groups into three of the Sn–N bonds of [Sn\{NMe$_2$\}$_2$]$_2$ to form a central seven-membered \{Sn$_2$N$_2$COC\} heterocycle in a distorted chair-like conformation, comprising of bridging \{$\mu$-NMe$_2$\} and \{$\mu$-*O,N*-OC(NMe$_2$)N-Ph\} units. Similar bridging of ureide ligands has been reported previously.[40] The remaining two ureide ligands coordinate to each of the two Sn(II) centers in a \{$\kappa$-*O,N*\} fashion. In all three ureide ligands the \{NMe$_2$\} groups adopt terminal positions '*exo*' to the heterocyclic core. Electronic delocalization in the \{NC(O)N\} part of the ureide ligand is evident from the relevant \{C–O\}

(ranged from 1.275(4) to 1.284(4) Å), and {C–N} bond lengths (1.313(5) to 1.345(4) Å) which are both in the range of partially double bond moieties, indicating that the π electrons of the ureide fragments are delocalized about the {NC(N)O} core. Significantly, while bond lengths within the bridging and terminal ureides are comparable, the {N-C-O} angle of the bridging ureide is substantially more obtuse [121.2(3)°] than comparable angles in the terminal ureides [115.3(3)° and 114.2(3)°].

**Table 3.** Selected bond lengths (Å) and angles (°) for complex **5**

| Bond lengths (Å) | | Bond Angles (°) | |
|---|---|---|---|
| Sn(1)-O(11) | 2.402(2) | O(11)-Sn(1)-O(21) | 139.12(9) |
| Sn(1)-O(21) | 2.233(2) | N(11)-Sn(1)-N(4) | 96.14(11) |
| Sn(1)-N(11) | 2.199(3) | O(11)-Sn(1)-N(4) | 83.45(9) |
| Sn(1)-N(4) | 2.197(3) | O(21)-Sn(1)-N(11) | 84.70(10) |
| Sn(2)-N(4) | 2.270(3) | O(11)-Sn(1)-N(11) | 57.36(10) |
| Sn(2)-N(21) | 2.236(3) | O(21)-Sn(1)-N(4) | 86.44(9) |
| Sn(2)-O(31) | 2.363(3) | | |
| Sn(2)-N(31) | 2.230(3) | O(31)-Sn(2)-N(21) | 122.87(10) |
| | | N(31)-Sn(2)-N(4) | 114.50(11) |
| O(11)-C(11) | 1.277(4) | O(31)-Sn(2)-N(4) | 77.44(10) |
| C(11)-N(11) | 1.345(4) | N(21)-Sn(2)-N(31) | 83.79(11) |
| C(11)-N(1) | 1.357(4) | O(31)-Sn(1)-N(31) | 56.38(10) |
| O(21)-C(21) | 1.284(4) | N(21)-Sn(2)-N(4) | 86.14(10) |
| C(21)-N(21) | 1.343(4) | | |
| C(21)-N(2) | 1.351(5) | O(11)-C(11)-N(11) | 115.3(3) |
| O(31)-C(31) | 1.274(4) | O(21)-C(21)-N(21) | 121.2(3) |
| C(31)-N(31) | 1.313(5) | O(31)-C(31)-N(31) | 114.2(3) |
| C(31)-N(3) | 1.343(18) | | |

As can be seen from Figure 6, the phenyl groups appended to the ureide ligands are orientated away from co-planarity with the {NC(O)N} plane and the N–C distances to the phenyl groups (1.402 to 1.416 Å) reflect typical values of single bonds. Mesomeric interactions of the nitrogen lone pairs, on the amido nitrogen atoms, with the aromatic rings can therefore be excluded. In contrast, the {NMe$_2$} groups on all three ureide ligands, are all approximately planar (Sum of angles about N: $\sum_N \sim 360°$) and tend towards to co-planarity with the {NC(O)} backbones in all three ligands in **1** [dihedral angles: O(11)-C(11)-N(1)-C(1) 4.43°, N(11)-C(11)-N(1)-C(2) 13.04°; O(22)-C(22)-N(2)-C(3) 8.13°, N(22)-C(22)-

N(2)-C(4) 25.51°; O(31)-C(31)-N(3)-C(5A) 21.39°, N(31)-C(31)-N(3)-C(6) 16.48°], suggestive of interaction between the {NMe$_2$} group and the {NCO} backbone.

The Sn–N bond lengths [Sn(1)-N(11) 2.198(3) Å; Sn(2)-N(21) 2.236(3) Å; Sn(2)-N(31) 2.230(3) Å] and Sn-O bond lengths [Sn(1)-O(11) 2.232(2) Å; Sn(1)-O(21) 2.232(2) Å; Sn(2)-O(31) 2.362(3) Å] are comparable to those of **1** and intermediate between the characteristic ranges of covalent Sn–N and Sn-O bonds and donor–acceptor interactions.

The precise reason for the formation of this *tri*-ureide compound **5**, rather than the desired *bis*-ureide system [Sn{κ$^2$*N,O*-PhNC(NMe$_2$)O}$_2$] which should be isostructural to **2** and **6**, is unknown. However repeated attempts to prepare the complex by the systematic addition of 1 to 4 equivalents of phenylisocyanate to [Sn(μ-NMe$_2$)(NMe$_2$)]$_2$ resulted in the isolation of crystals consisting of the bimetallic *tri*-ureide, **5**.

## Thermogravimetric analysis of compounds 2, 3 and 4

Precursor requirements for MOCVD centre around thermal stability, volatility, and clean thermal decomposition to the desired material, ideally at low temperatures. For ALD, greater emphasis is placed on high volatility and thermal stability at the operating temperature of the process to ensure thermal decomposition does not take place.[41, 42] Thermogravimetric analysis (TGA) was employed to investigate the volatility and thermal stability of complexes **2**, **3**, **4** and **6** to assess their potential utility within these techniques. These analyses were carried out with an instrument housed in a nitrogen filled purge-box in order to minimize reaction with atmospheric moisture/air. Figure 7 shows the thermal profiles, as determined by TGA, of complexes **2**, **3**, **4** and **6**, and Table 4 reports the expected % residue, % of non-volatile residue and onset of volatilisation/decomposition for complexes **2**-**4** and **6**. We have previously described the suitability of compound **3** for the AACVD of SnO.[17] That data is included here for comparative reasons. Thermogravimetric analysis (TGA) was therefore performed on compounds **2**, **4** and **6**. Complexes **1** and **5** were not examined by TGA due to their room temperature instability and molecular structure respectively.
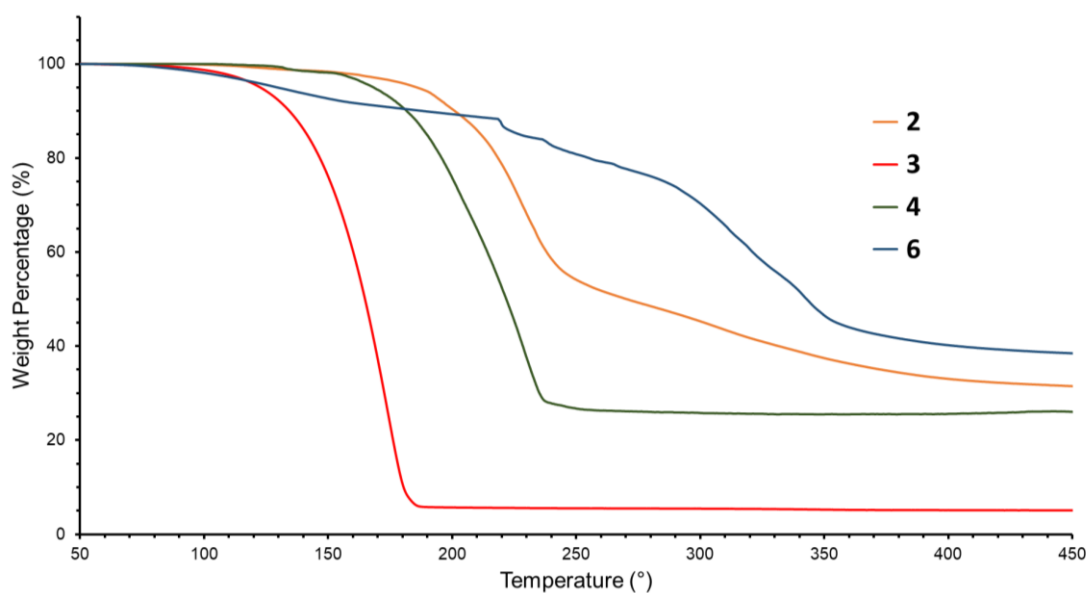
**Figure 7:** Thermogravimetric analysis plot of data for complexes **2**, **3**, **4** and **6**. Experiments were run under $N_2$ (50 mL/min) at a ramp rate of 5 °C/min between 30–500 °C.

**Table 4:** Expected % residue, % of non-volatile residue and onset of volatilisation/decomposition for complexes **2**-**4** and **6**.

| Precursor | Expected % for $SnO_2$, SnO or Sn | % Non-volatile Residue (Temp.) | Onset Temp.[§] |
|:---:|:---:|:---:|:---:|
| **2** | 33.1%, 29.0 % & 26.0 % | 32.0 % (428 °C) | 128 °C |
| **3**[17] | 37.4%, 33.0 % & 29.5 % | 5.7 % (190.0 °C) | 96 °C |
| **4** | 27.0%, 24.2% & 31.3 % | 26.5 % (253 °C) | 129°C |
| **6** | 28.61%, 25.6 % & 22.6 % | 36.0 % (550°C) No stable ressidue formed | 87 °C |

[§] The temperature at which 1% mass loss has occurred

The TGA of compounds **3** and **4** clearly show single mass loss events with onset temperatures of 96 °C and 129 °C, respectively. In the case of **3**, a stable residue was obtained at 190 °C (5.7%) with <0.5 % further mass loss to a high temperature limit of 525 °C, which provided a residual mass of *ca.* 5%, considerably lower than expected for neither $SnO_2$ (37.4%), SnO (33.4 %) or tin metal (29.5 %). Contrastingly, complex **4** forms a stable residue at *ca.* 253 °C (26.5%) with no further mass loss. While the residual mass formed from **4** is between values calculated for the formation of pure $SnO_2$ (27.0 %) and SnO (24.2 %), it is higher than the calculated residual mass for the formation of tin metal (21.3%).

Although the results will not be repeated here, we have previously described the suitability of compound **3** for aerosol-assisted chemical vapour deposition (AACVD) for film growth studies.[17]

The TGA trace and its corresponding derivatives for compounds **2** and **6** indicate complex decomposition pathways. While the TGA trace for **2** is less convoluted than that of complex **6**, the trace indicates several distinct mass loss events starting with an onset of decomposition at *ca.* 127 °C, with what appears to be a single mass loss, corresponding to *ca.* 46% of the original mass (between 127–245 °C). A possible cause of this mass loss is the incomplete de-insertion of the cyclohexyl isocyanate moieties, to form $[Sn(NMe_2)_2]$, which would result in a mass loss of up to 54%. With increasing temperatures, *i.e.* between 245–433 °C, several continuous mass loss events follow, resulting in a stable mass residue of 32.0 % at 428.3 °C; a value which is higher than that calculated for the formation of tin metal (26.0 %), but is between values calculated for the formation of either $SnO_2$ (33.1 %) or SnO (29.0%).

In the case of **6** the TGA trace displays several distinct mass loss events during the decomposition, from 86 °C through to 400 °C. Although the weight percentage began to stabilise at this temperature, mass loss was still recorded up to the cessation of the analysis at 550 °C. The residual mass at this temperature (36%) corresponded neither with $SnO_2$ (28.6 %), SnO (25.6 %) nor with tin metal (22.6 %) indicating that this compound holds little potential for oxidation state control or stoichiometry control as a single source precursor to either SnO or $SnO_2$.

Attempts to elucidate the decomposition pathways of **2**-**4** and **6** through TGA-MS experiments were inconclusive, partly because of the air sensitivity of the complexes. In the case of complexes **3** and **6** however, peaks at m/z = 45.05 amu were observed in the mass spectra, which we attribute to formation of dimethyl amine. Attempts to analyse TGA pan residues by analysis of powder X-ray diffraction patterns were unsuccessful, with only Bragg peaks at 38.5° and 44.4° corresponding the to (111) and (200) planes of Aluminium metal (from the TGA pans) present in the plots.

## Conclusions

As part of a continuing effort to optimize the development of precursors and to the identify properties of a precursor complex, which provide ideal volatility, reactivity and stability, we have demonstrated the feasibility of ureide ligands as stabilizing ligands in precursor chemistry by synthesizing a series of new tin(II) complexes. These complexes were synthesized by the direct insertion of $[Sn(NMe_2)_2]_2$ reactions with a range of isocyanate ligands to for the corresponding Sn(II) ureide complexes. The molecular structures of **2**, **3**, **4** and **6** showed that these systems formed as monomers in which the central metal atoms are tetracoordinate with pseudo trigonal-bipyramidal or square based pyramidal

geometries. In the case of complexes **2** and **6**, bearing the cyclohexyl and mesityl derivatized ureide ligands the complexes display molecular $C_2$ symmetry bearing $\kappa^2$-N,O coordinated ligands. Based on $^{119}$Sn{$^1$H} NMR spectroscopy we assume that the unstable isopropyl derivative, **1**, possess a comparable structure to complexes **2** and **6**. In the case of complexes **3** and **4** the molecular $C_2$ symmetry is broken, with the complexes in the solid-state possessing two ureide ligands which display $\kappa^2$-N,O and $\kappa^2$-N,N' coordination. TGA analysis of the complexes **2**, **3**, **4** and **6** shows varying behavior, with complexes **3** and **4** both of which display ambivalent coordination of the ureide ligands in the solid state, displaying single mass loss events. In the case of **3**, residual masses ca. 6%, significantly lower than that expected for formation of SnO (33%), indicate a significant degree of volatility for the complex, indicative of its possible utility in ALD. TGA of **4** provides a residual mass of 26.5%, close to that expected for SnO formation (24.2%), indicating a reduced volatility but potential utility of **4** in the AACVD of SnO thin films. In contrast, complexes **2** and **6** which display only display $\kappa^2$-N,O coordination of the ureide ligand in the solid state, are significantly less volatile and display complicated decomposition profiles.

## Experimental

All reactions dealt with potentially air- and moisture-sensitive compounds, and as such, were carried out under an argon atmosphere using standard Schlenk line and glovebox techniques in an MBraun Labmaster glovebox at $O_2$, $H_2O$ < 2.5 ppm. NMR experiments were conducted in Youngs tap NMR tubes prepared and sealed in a glovebox under argon and were recorded on a Bruker AV-300 at 75.5 MHz. The spectra were referenced relative to residual solvent resonances. Unless otherwise stated data quoted was recorded at 298 K. Elemental analysis was performed by Mr. Stephen Boyer at SACS, London Metropolitan University. Solvents for air- and moisture-sensitive reactions were provided by an Innovative Technology Solvent Purification System, or dried/degassed manually according to established laboratory procedures. $Sn(NMe_2)_2$ was produced according to literature procedures.[43] All other reagents were purchased from commercial sources and used without further purification.

***Synthesis of Tin(II) bis-N-iso-propyl-N',N'-dimethylureide*** (**1**). Isopropyl isocyanate (165 mg, 1.94 mmol) was added to a stirred solution (10 ml, toluene) of $Sn(NMe_2)_2$ (200 mg, 0.97mmol). After 30 mins reaction time solvent removal in vacuo resulted in the isolation of an orange oil which showed signs of decomposition. NMR analysis of the reaction solution was, however, consistent with the formation of the desired product. $^1$H NMR (300MHz, $C_7H_8$); δ 1.23-1.25 (br m, 6H, CH<u>Me</u>$_2$), 2.57 (s,

6H, N$\underline{\text{Me}}_2$), 3.89-4.01 (m, 1H, C$\underline{\text{H}}$Me$_2$). $^{13}$C{$^1$H} NMR (75 MHz, C$_6$H$_6$); δ 25.3 (CH$\underline{\text{Me}}_2$), 39.0 (N$\underline{\text{Me}}_2$), 47.2 ($\underline{\text{C}}$HMe$_2$), 167.2 (N$\underline{\text{C}}$(O)N). $^{119}$Sn{$^1$H} NMR (112 MHz, C$_7$H$_8$); δ −307.0

***Synthesis of Tin(II) bis-N-cyclohexyl-N',N'-dimethylureide*** (**2**). Cyclohexyl isocyanate (243 mg, 1.94 mmol) was added to a stirred solution (10 ml, toluene) of Sn(NMe$_2$)$_2$ (200 mg, 0.97mmol) at room temperature. After 30 mins reaction time solvent removal in vacuo resulted in the isolation of a cream off-white solid. Extraction into fresh toluene (5ml), followed by filtration through celite to remove insoluble residues and storage at −5 °C, resulted in the formation of pale-yellow crystals, which were isolated by filtration and washed with cold hexanes. Yield: 346 mg, 78%. Analysis found (%) (calc. for C$_{18}$H$_{34}$N$_4$O$_2$Sn): C 47.4 (47.3), H 7.36 (7.50), N 12.0 (12.3). $^1$H NMR (300 MHz, C$_7$H$_8$); δ 1.10-1.20 (m, 1H, C$\underline{\text{H}}_2$), 1.52-1.75 (m, 6H, C$\underline{\text{H}}_2$), 1.84-1.95 (m, 2H, C$\underline{\text{H}}_2$), 2.59 (s, 6H, N$\underline{\text{Me}}_2$), 3.45-3.60 (m, 1H, C$\underline{\text{H}}$). $^{13}$C{$^1$H} NMR (74 MHz, C$_7$H$_8$); δ 26.2 (s, $\underline{\text{C}}$H$_2$), 26.3 ($\underline{\text{C}}$H$_2$), 35.6 ($\underline{\text{C}}$H$_2$), 38.6 (br s, N$\underline{\text{Me}}_2$), 55.3 (s, $\underline{\text{C}}$H), 166.8 (s, N$\underline{\text{C}}$(O)N). $^{119}$Sn{$^1$H} NMR (112 MHz, C$_7$H$_8$); δ −310.

***Synthesis of Tin(II) bis-N-tertbutyl-N',N'-dimethylureide*** (**3**).[17] Following the same procedure for the synthesis of **1**, t-Butyl isocyanate (192 mg, 1.94 mmol) was reacted with Sn(NMe$_2$)$_2$ (200 mg, 0.97mmol). Extraction into fresh toluene (5ml), followed by filtration through celite to remove insoluble residues and storage at −5 °C, resulted in the formation of pale-yellow crystals, which were isolated by filtration and washed with cold hexanes. Yield: 346 mg, 78%. Analysis found (%) (calc. for C$_{14}$H$_{30}$N$_4$O$_2$Sn): C 41.5 (41.5), H 7.5 (7.5), N 13.7 (13.8). $^1$H NMR (300 MHz, C$_7$H$_8$); δ 1.37 (br s, 9H, C(C$\underline{\text{H}}_3$)$_3$, 2.44 (s, 6H, N$\underline{\text{Me}}_2$). $^{13}$C{$^1$H} NMR (74 MHz, C$_7$H$_8$); δ 31.4 (s, C($\underline{\text{C}}$H$_3$)$_3$), 41.4 (br s, N$\underline{\text{Me}}_2$), 53.0 (s, $\underline{\text{C}}$(CH$_3$)$_3$), 166.9 (s, N$\underline{\text{C}}$(O)N). $^{119}$Sn{$^1$H} NMR (112 MHz, C$_7$H$_8$); δ −357.

***Synthesis of Tin(II) bis-N-adamantyl-N',N'-dimethylureide*** (**4**). Following the same procedure for the synthesis of **1**, adamantyl isocyanate (343 mg, 1.94 mmol) was reacted with Sn(NMe$_2$)$_2$ (200 mg, 0.97mmol). Extraction into fresh toluene (5ml), followed by filtration through celite to remove insoluble residues and storage at −25 °C, resulted in the formation of colourless crystal, which were isolated by filtration and washed with cold hexanes. Yield: 414 mg, 76%. Analysis found (%) (calc. for C$_{26}$H$_{42}$N$_4$O$_2$Sn): C 55.34 (55.63), H 7.41 (7.55), N 10.05 (9.98). $^1$H NMR (300 MHz, C$_7$H$_8$); δ 1.56 (br m, 6H, C$\underline{\text{H}}_2$), 1.93 (br m, 3H, C$\underline{\text{H}}$), 2.07 (m, 6H, C$\underline{\text{H}}_2$), 2.39 (s, 6H, N$\underline{\text{Me}}_2$). $^{13}$C{$^1$H} NMR (74 MHz, C$_7$H$_8$); δ 30.3 ($\underline{\text{C}}$H$_2$), 36.8 (N$\underline{\text{Me}}_2$), 42.9 ($\underline{\text{C}}$H$_2$), 44.2 ($\underline{\text{C}}$H), 57.6 (s, $\underline{\text{C}}$H), 166.4 (s, N$\underline{\text{C}}$(O)N). $^{119}$Sn{$^1$H} NMR (112 MHz, C$_7$H$_8$); δ −353.

***Synthesis of dimethylamido-ditin(II) tris-N-Phenyl-N',N'-dimethylureide*** (**5**). Phenyl isocyanate (462 mg, 3.88 mmol) was added dropwise, over 10 min, to a cooled (−40 °C) and stirred THF solution (15 mL) of Sn(NMe$_2$)$_2$ (200 mg, 0.97 mmol). After stirring at room temperature for 2 h, THF was removed *in vacuo*. To the residual solid, 15 mL of hexane was added and stirred for 20 min. After filtration through Celite. The solution was stored at RT for 3 days, during which time colourless crystalline

needles were formed. The product was subsequently isolated by filtration and dried *in vacuo*. Yield: 224 mg, 60 %. Analysis found (%) (calc. for $C_{29}H_{39}N_7O_3Sn_2$): C, 45.24 (45.17); H, 4.88 (5.10); N, 11.75 (12.72). $^1H$ NMR (300 MHz, $C_6D_6$): δ 2.27 (br. s, 12H, N<u>Me</u>₂), 2.32-2.80 (br. m, 12H, N<u>Me</u>₂), 6.76-6.85 (m, 3H, *p*-C<u>H</u>), 6.89-6.99 (m, 6H *o*-C<u>H</u>), 7.05-7.13 (m, 6H, m-C<u>H</u>); $^{13}C\{^1H\}$ NMR (75.5 MHz, $C_6D_6$-d⁶): δ 38.2 (br. s, N<u>Me</u>₂), 40.0 (br. s, μ-N<u>Me</u>₂), 121.8 (s, Ar-<u>C</u>H), 124.4 (s, Ar-<u>C</u>H), 128.9 (Ar-<u>C</u>H), 147.3 (s, ipso-<u>C</u>), 164.9 (s, N<u>C</u>(O)N); $^{119}Sn\{^1H\}$ [$^1H$] NMR (112 MHz, $C_6D_6$-d⁶): $δ_{Sn}$ −217 (s).

*Synthesis of Tin(II) bis-N-mesityl-N',N'-dimethylureide* (**6**). Following the same procedure for the synthesis of **1**, mesityl isocyanate (272mg, 1.94mmol) was added to a solution of Sn(NMe₂)₂ (200 mg, 0.97mmol) in toluene (10mL). Extraction into fresh toluene (5ml), followed by filtration through celite to remove insoluble residues and storage at 0 °C, resulted in the formation of large colourless crystal, which were isolated by filtration and washed with cold hexanes. Yield: 503 mg, 98 %. Analysis found (%) (calc. for $C_{24}H_{34}N_4O_2Sn$): C 54.4 (54.5), H 6.57 (6.48), N 10.6 (10.6). $^1H$ NMR (300 MHz, $C_7D_8$); δ 2.17 (s, 3H, *p*-<u>Me</u>), 2.35 (s, 6H, *o*-<u>Me</u>) 2.37 (s, 6H, N<u>Me</u>₂), 6.75 (s, 2H, Ar-C<u>H</u>). $^{13}C\{^1H\}$ NMR (75.5 MHz, $C_7D_8$); δ 19.4 (s, *p*-<u>Me</u>), 20.9 (s, *o*-<u>Me</u>), 36.5 (s, N<u>Me</u>₂), 132.7 (s, *p*-<u>C</u>Me) 133.9 (s, *m*-<u>C</u>H), 137.4 (*o*-<u>C</u>Me), 141.1 (s, *ipso*-<u>C</u>), 164.4 (N<u>C</u>(O)N). $^{119}Sn\{^1H\}$ NMR (112 MHz, $C_7D_8$); δ −353.1

**Single Crystal X-ray Diffraction**:

Experimental details relating to the single-crystal X-ray crystallographic studies for compounds **2-6** are summarised in Table 5. All crystallographic data were collected at 150(2)K on a SuperNova, Dual, EosS2 diffractometer using radiation Cu-Kα (λ= 1.54184 Å) or Mo-Kα (λ= 0.71073 Å). All structures were solved by direct methods followed by full-matrix least squares refinement on F2 using the WINGX-2014 suite of programs[44] or OLEX2.[45] All hydrogen atoms were included in idealised positions and refined using the riding model. Crystals were isolated from an argon-filled Schlenk flask and immersed under oil before being mounted onto the diffractometer.

**Table 5:** X-ray Crystallographic Data for Compounds **2-6**.

| Compound | **2** | **3**[17] | **4** | **5** | **6** |
|---|---|---|---|---|---|
| Chemical formula | $C_{18}H_{34}N_4O_2Sn$ | $C_{14}H_{30}N_4O_2Sn$ | $C_{26}H_{42}N_4O_2Sn$ | $C_{29}H_{39}N_7O_3Sn_2$ | $C_{24}H_{34}N_4O_2Sn$ |
| Formula Mass | 457.18 | 405.11 | 561.32 | 771.05 | 529.24 |
| Crystal system | Monoclinic | Triclinic | Monoclinic | Triclinic | Triclinic |
| Space group | $P2_1/n$ | $P\bar{1}$ | $P2_1/n$ | $P\bar{1}$ | $P\bar{1}$ |
| $a$/Å | 9.0643(3) | 8.6700(3) | 10.4406(4) | 9.4500(5) | 11.1330(5) |
| $b$/Å | 24.4486(8) | 9.4020(3) | 11.5708(5) | 11.6707(6) | 11.2160(5) |
| $c$/Å | 9.9477(4) | 12.4160(3) | 21.5541(9) | 16.5204(8) | 12.4200(4) |
| $\alpha$/° | 90 | 79.878(2) | 90 | 71.124(5) | 101.829(2) |
| $\beta$/° | 109.0738(16) | 84.754(2) | 93.010(4) | 75.263(5) | 105.225(2) |
| $\gamma$/° | 90 | 70.462(2) | 90 | 67.938(5) | 117.416(2) |
| Unit cell volume/Å$^3$ | 2083.47(13) | 938.39(5) | 2600.27(19) | 1579.34(16) | 1228.44(9) |
| Temperature/K | 150(2) | 150(2) | 150(2) | 150(2) | 150(2) |
| $Z$ | 4 | 2 | 4 | 2 | 2 |
| No. of reflections measured | 31337 | 14456 | 20833 | 13364 | 24165 |
| No. of independent reflections | 6081 | 5596 | 5334 | 7074 | 6579 |
| $R_{int}$ | 0.0954 | 0.0340 | 0.0724 | 0.0412 | 0.0549 |
| Final $R_1$ values ($I > 2\sigma(I)$) | 0.0448 | 0.0228 | 0.0613 | 0.0400 | 0.0334 |
| Final $wR(F^2)$ values ($I > 2\sigma(I)$) | 0.0718 | 0.0539 | 0.1127 | 0.0642 | 0.0740 |
| Final $R_1$ values (all data) | 0.1194 | 0.0272 | 0.1053 | 0.0569 | 0.0462 |
| Final $wR(F^2)$ values (all data) | 0.0880 | 0.0556 | 0.1268 | 0.0727 | 0.0797 |
| Goodness of fit on $F^2$ | 0.965 | 1.044 | 1.126 | 1.030 | 1.050 |
| CCDC number | 1916466 | 952206 | 2100178 | 1916467 | 1916465 |

**Thermogravimetric Analysis (TGA):** TGA was collected using a TGA 4000 Perkin Elmer system, housed in an argon-filled glovebox. Samples were prepared air sensitively, and TGAs were performed under a flow of Ar at 20 ml min-1 and heated from 30 °C to 500 °C at a ramp rate of 5 °C min-1.

**Accession Codes**

CCDC 952206, 1916465-67 and 2100178 contain the supplementary crystallographic data for this paper. These data can be obtained free of charge via www.ccdc.cam.ac.uk/data_request/cif, or by emailing data_request@ccdc.cam.ac.uk, or by contacting The Cambridge Crystallographic Data Centre, 12 Union Road, Cambridge CB2 1EZ, UK; fax: +44 1223 336033.

**Corresponding Authors**

Andrew L. Johnson - Department of Chemistry, University of Bath, Claverton Down, Bath BA2 7AY, United Kingdom; http://orcid.org/0000-0001-5241-0878; Email: A.L.Johnson@bath.ac.uk

**Authors**

Thomas Wildsmith - Department of Chemistry, University of Bath, Claverton Down, Bath BA2 7AY, United Kingdom; Centre for Sustainable Chemical Technologies, University of Bath, Bath BA2 7AY, United Kingdom.

James D. Parish - Department of Chemistry, University of Bath, Claverton Down, Bath BA2 7AY, United Kingdom; http://orcid.org/ 0000-0003-1138-3820

Ibbi Y. Ahmet - Department of Chemistry, University of Bath, Claverton Down, Bath BA2 7AY, United Kingdom; Centre for Sustainable Chemical Technologies, University of Bath, Bath BA2 7AY, United Kingdom; http://orcid.org/ 0000-0003-0986-1950

Kieran C. Molloy - Department of Chemistry, University of Bath, Claverton Down, Bath BA2 7AY, United Kingdom; http://orcid.org/ 0000-0001-7346-7427

Michael S. Hill - Department of Chemistry, University of Bath, Claverton Down, Bath BA2 7AY, United Kingdom; http://orcid.org/ 0000-0001-9784-9649

**Author Contributions**

The manuscript was written through contributions of all authors. All authors have given approval to the final version of the manuscript.

**Conflicts of interest**

There are no conflicts to declare.

# References

1. Eds: Kasap, S.; Capper, P. *Springer Handbook of Electronic and Photonic Materials,* Springer, Cham: 2017, DOI: 10.1007/978-3-319-48933-9.

2. Fortunato, E.; Barquinha, P.; Martins, R. Oxide Semiconductor Thin-Film Transistors: A Review of Recent Advances. *Adv. Mater.,* **2012,** 24 (22), 2945-2986, DOI: 10.1002/adma.201103228.

3. Hautier, G.; Miglio, A.; Ceder, G.; Rignanese, G.-M.; Gonze, X. Identification and design principles of low hole effective mass p-type transparent conducting oxides, *Nat. Commun.,* **2013,** 4 (1), DOI: 10.1038/ncomms3292.

4. Wang, Z.; Nayak, P. K.; Caraveo-Frescas, J. A.; Alshareef, H. N. Recent Developments in p-Type Oxide Semiconductor Materials and Devices, *Adv. Mater.,* **2016,** 28 (20), 3831-3892, DOI: 10.1002/adma.201503080.

5. Yim, K.; Youn, Y.; Lee, M.; Yoo, D.; Lee, J.; Cho, S. H.; Han, S. Computational discovery of p-type transparent oxide semiconductors using hydrogen descriptor, *Npj Comput. Mater.,* **2018,** 4 (17), DOI: 10.1038/s41524-018-0073-z.

6. Hosono, H.; Ogo, Y.; Yanagi, H.; Kamiya, T. Bipolar Conduction in SnO Thin Films, *Electrochem. Solid St.,* **2011,** 14 (1), Ii13-Ii16, DOI: 10.1149/1.3505288.

7. Saji, K. J.; Tian, K.; Snure, M.; Tiwari, A. 2D Tin Monoxide-An Unexplored p-Type van der Waals Semiconductor: Material Characteristics and Field Effect Transistors, *Adv. Electron. Mate.,* **2016,** 2 (4), 1500453, DOI: 10.1002/aelm.201500453.

8. Guo, W.; Fu, L.; Zhang, Y.; Zhang, K.; Liang, L. Y.; Liu, Z. M.; Cao, H. T.; Pan, X. Q. Microstructure, optical, and electrical properties of p-type SnO thin films, *Appl. Phys. Lett.,* **2010,** 96 (4) 042113, DOI: 10.1063/1.3277153.

9. Nomura, K.; Kamiya, T.; Hosono, H. Ambipolar Oxide Thin-Film Transistor, *Adv. Mater.* **2011,** 23 (30), 3431-3434, DOI: 10.1002/adma.201101410.

10. Ogo, Y.; Hiramatsu, H.; Nomura, K.; Yanagi, H.; Kamiya, T.; Hirano, M.; Hosono, H. p-channel thin-film transistor using p-type oxide semiconductor, SnO. *App. Phys. Lett.,* **2008,** 93 (3) 032113, DOI: 10.1063/1.2964197.

11. Ogo, Y.; Hiramatsu, H.; Nomura, K.; Yanagi, H.; Kamiya, T.; Kimura, M.; Hirano, M.; Hosono, H. Tin monoxide as an s-orbital-based p-type oxide semiconductor: Electronic structures and TFT application, *Phys. Status solidi A,* **2009,** 206 (9), 2187-2191 DOI: 10.1002/pssa.200881792.

12. Toyama, T.; Seo, Y.; Konishi, T.; Okamoto, H.; Tsutsumi, Y. Physical Properties of p-Type Tin Monoxide Films Deposited at Low Temperature by Radio Frequency Magnetron Sputtering, *Appl. Phys. Express,* **2011,** 4 (7), 071101, DOI: 10.1143/apex.4.071101.

13. Sanal, K. C.; Jayaraj, M. K. Growth and characterization of tin oxide thin films and fabrication of transparent p-SnO/n-ZnO p–n hetero junction, *Mater. Sci. Eng. B,* **2013,** 178 (12), 816-821 DOI: 10.1016/j.mseb.2013.04.007.

14. Yabuta, H.; Kaji, N.; Hayashi, R.; Kumomi, H.; Nomura, K.; Kamiya, T.; Hirano, M.; Hosono, H. Sputtering formation of p-type SnO thin-film transistors on glass toward oxide complimentary circuits, *Applied Physics Letters* **2010,** 97 (7), 072111, DOI: 10.1063/1.3478213.

15. Barbul, I.; Johnson, A. L.; Kociok-Köhn, G.; Molloy, K. C.; Silvestru, C.; Sudlow, A. L. The Reaction and Materials Chemistry of [$Sn_6(O)_4(OSiMe_3)_4$]: Chemical Vapour Deposition of Tin Oxide, *ChemPlusChem* **2013,** 78 (8), 866-874, DOI: 10.1002/cplu.201300104.

16. Hill, M. S.; Johnson, A. L.; Lowe, J. P.; Molloy, K. C.; Parish, J. D.; Wildsmith, T.; Kingsley, A. L. Aerosol-assisted CVD of SnO from stannous alkoxide precursors, *Dalton Trans.,* **2016,** 45 (45), 18252-18258, DOI: 10.1039/c6dt02508k.

17. Wildsmith, T.; Hill, M. S.; Johnson, A. L.; Kingsley, A. J.; Molloy, K. C. Exclusive formation of SnO by low temperature single-source AACVD, *Chemical Commun.,* **2013,** 49 (78), 8773-8775, DOI: 10.1039/c3cc45676e.

18. Han, J. H.; Chung, Y. J.; Park, B. K.; Kim, S. K.; Kim, H.-S.; Kim, C. G.; Chung, T.-M. Growth of p-Type Tin(II) Monoxide Thin Films by Atomic Layer Deposition from Bis(1-dimethylamino-2-methyl-2propoxy)tin and $H_2O$, *Chem. Mater.* **2014,** 26 (21), 6088-6091, DOI: 10.1021/cm503112v.

19. Kim, H. Y.; Nam, J. H.; George, S. M.; Park, J.-S.; Park, B. K.; Kim, G. H.; Jeon, D. J.; Chung, T.-M.; Han, J. H. Phase-controlled $SnO_2$ and SnO growth by atomic layer deposition using Bis(N-ethoxy-2,2-dimethyl propanamido)tin precursor, *Ceram. Int.,* **2019,** 45 (4), 5124-5132, DOI: 10.1016/j.ceramint.2018.09.263.

20. George, S. M.; Nam, J. H.; Lee, G. Y.; Han, J. H.; Park, B. K.; Kim, C. G.; Jeon, D. J.; Chung, T.-M. N-Alkoxy Carboxamide Stabilized Tin(II) and Germanium(II) Complexes for Thin-Film Applications, *Eur. J. Inorg. Chem.,* **2016,** 2016 (36), 5539-5546, DOI: 10.1002/ejic.201600884.

21. Kim, H.-M.; Choi, S.-H.; Jeong, H. J.; Lee, J.-H.; Kim, J.; Park, J.-S. Highly Dense and Stable p-Type Thin-Film Transistor Based on Atomic Layer Deposition SnO Fabricated by Two-Step Crystallization, *ACS Appl. Mater. Interfaces,* **2021,** 13 (26), 30818-30825, DOI: 10.1021/acsami.1c06038.

22. Catherall, A. L.; Hill, M. S.; Johnson, A. L.; Kociok-Köhn, G.; Mahon, M. F. Homoleptic Zirconium Amidates: Single Source Precursors for the Aerosol-assisted Chemical Vapour Deposition of $ZrO_2$, *J. Mater. Chem. C,* **2016,** 4 (45), 10731-10739, DOI: 10.1039/c6tc03631g.

23. Pothiraja, R.; Milanov, A. P.; Barreca, D.; Gasparotto, A.; Becker, H.-W.; Winter, M.; Fischer, R. A.; Devi, A. Hafnium carbamates and ureates: new class of precursors for low-temperature growth of HfO2 thin films, *Chem. Commun.,* **2009,** (15), 1978-1980, DOI: 10.1039/b821128k.

24. Alves, L. G.; Madeira, F.; Munhá, R. F.; Barroso, S.; Veiros, L. F.; Martins, A. M. Reactions of heteroallenes with cyclam-based Zr(iv) complexes, *Dalton Trans.,* **2015,** 44 (3), 1441-1455, DOI: 10.1039/c4dt02851a.

25. Lavoie, N.; Ong, T.-G.; Gorelsky, S. I.; Korobkov, I.; Yap, G. P. A.; Richeson, D. S. Bis(imido) W(VI) Complexes Chelated by N,N'-Disubstituted 1,8-Diamidonaphthalene: An Analysis of Bonding, Isocyanate Insertion, and Al-Me Transfer, *Organometallics,* **2007,** 26 (26), 6586-6590, DOI: 10.1021/om700763v.

26. Cotton, F. A.; Ilsley, W. H.; Kaim, W. Sensitivity of the chromium-chromium quadrupole bond to axial interactions in dichromium(II) compounds, *J. Am. Chem. Soc.,* **2002,** 102 (10), 3464-3474, DOI: 10.1021/ja00530a026.

27. Gupta, R.; Zhang, Z. H.; Powell, D.; Hendrich, M. P.; Borovik, A. S. Synthesis and Characterization of Completely Delocalized Mixed-Valent Dicopper Complexes, *Inorg. Chem.,* **2002,** 41 (20), 5100-5106, DOI: 10.1021/ic0202918.

28. Payne, P. R.; Bexrud, J. A.; Leitch, D. C.; Schafer, L. L. Asymmetric hydroamination catalyzed by in situ generated chiral amidate and ureate complexes of zirconium — Probing the role of the tether in ligand design, *Can. J. Chem.,* **2011,** 89 (10), 1222-1229, DOI: 10.1139/v11-091.

29. Liu, R.; Li, Z.; Yi, W.; Chen, Z.; Zhou, X. Reactivity of lanthanocene hydroxides toward carbodiimide and $CO_2$: Synthesis and characterization of lanthanide ureido and carbonate complexes, *J. Organomet. Chem.,* **2011,** 696 (13), 2648-2653, DOI: 10.1016/j.jorganchem.2011.04.016.

30. Bradley, D. C.; Hursthouse, M. B.; Jelfs, A. N. d. M.; Short, R. L. A novel trinuclear organoimido vanadium(V) compound. Crystal and molecular structure of $[V_3Cl_2(NBu^t)_3(\mu^2\text{-}NPh)_3(\mu^3\text{-}PhNCONHBu^t)]$, *Polyhedron,* **1983,** 2 (8), 849-852, DOI: 10.1016/s0277-5387(00)87217-4.

31. Willcocks, A. M.; Pugh, T.; Hamilton, J. A.; Johnson, A. L.; Richards, S. P.; Kingsley, A. J. CVD of pure copper films from novel iso-ureate complexes, *Dalton Trans.,* **2013,** 42 (15), 5554-5565, DOI: 10.1039/c3dt00104k.

32. Ahmet, I. Y.; Hill, M. S.; Johnson, A. L.; Peter, L. M. Polymorph-Selective Deposition of High Purity SnS Thin Films from a Single Source Precursor, *Chem. Mater.,* **2015,** 27 (22), 7680-7688, DOI: 10.1021/acs.chemmater.5b03220.

33. Sullivan, H. S. I.; Parish, J. D.; Thongchai, P.; Kociok-Köhn, G.; Hill, M. S.; Johnson, A. L. Aerosol-Assisted Chemical Vapor Deposition of ZnS from Thioureide Single Source Precursors, *Inorg. Chem.,* **2019,** 58 (4), 2784-2797, DOI: 10.1021/acs.inorgchem.8b03363.

34. Bhide, M. A.; Mears, K. L.; Carmalt, C. J.; Knapp, C. E. Synthesis, solution dynamics and chemical vapour deposition of heteroleptic zinc complexes via ethyl and amide zinc thioureides. *Chemical Science* **2021,** 12 (25), 8822-8831 DOI: 10.1039/d1sc01846a.

35. Stewart, C. A.; Dickie, D. A.; Moasser, B.; Kemp, R. A. Reactions of $CO_2$ and related heteroallenes with $CF_3$-substituted aromatic silylamines of tin, *Polyhedron,* **2012,** 32 (1), 14-23, DOI: 10.1016/j.poly.2011.06.010.

36. Addison, A. W.; Rao, T. N.; Reedijk, J.; van Rijn, J.; Verschoor, G. C. Synthesis, structure, and spectroscopic properties of copper(II) compounds containing nitrogen–sulphur donor ligands; the crystal and molecular structure of aqua[1,7-bis(N-methylbenzimidazol-2'-yl)-2,6-dithiaheptane]copper(II) perchlorate, *J. Chem. Soc., Dalton Trans.* **1984,** (7), 1349-1356, DOI: 10.1039/dt9840001349.

37. Parish, J. D.; Snook, M. W.; Johnson, A. L.; Kociok-Köhn, G. Synthesis, characterisation and thermal properties of Sn(ii) pyrrolide complexes, *Dalton Trans.,* **2018,** 47 (23), 7721-7729, DOI: 10.1039/c8dt00490k.

38. Ruiz, J.; Rodríguez, V.; Vicente, C.; Pérez, J.; López, G.; Chaloner, P. A.; Hitchcock, P. B. Ureato(1−) complexes of palladium(II) and platinum(II),. *Inorg. Chim. Acta,* **2003,** 351, 114-118, DOI: 10.1016/s0020-1693(03)00200-7.

39. Alves, L. G.; Martins, A. M. Cyclam Functionalization through Isocyanate Insertion in Zr–N Bonds. *Inorg. Chem.,* **2011,** 51 (1), 10-12, DOI: 10.1021/ic201750y.

40. Uhl, W.; Tannert, J.; Layh, M.; Hepp, A.; Grimme, S.; Risthaus, T. Cooperative Ge–N Bond Activation in Hydrogallation Products of Alkynyl(diethylamino)germanes $(Et_2N)_nGe(C≡C^tBu)_{4−n}$, *Organometallics,* **2013,** 32 (22), 6770-6779, DOI: 10.1021/om400543v.

41. Devi, A. 'Old Chemistries' for new applications: Perspectives for development of precursors for MOCVD and ALD applications. *Coord. Chem. Rev.,* **2013,** 257 (23-24), 3332-3384, DOI: 10.1016/j.ccr.2013.07.025.

42. Dussarrat, C. Design, Synthesis and ALD Assessment of Organometallic Precursors for Semiconductor Applications, *ECS Trans.,* **2014,** 64 (9), 233-241, DOI: 10.1149/06409.0233ecst.

43. Fjeldberg, T.; Hope, H. k.; Lappert, M. F.; Power, P. P.; Thorne, A. J. Molecular structures of the main group 4 metal(II) bis(trimethylsilyl)-amides $M[N(SiMe_3)_2]_2$ in the crystal (X-ray) and vapour (gas-phase electron diffraction). *J. Chem. Soc., Chem. Comm.,* **1983,** (11), 639-641, DOI: 10.1039/c39830000639.

44. Farrugia, L. J. WinGXsuite for small-molecule single-crystal crystallography, *J. Appl. Crystallog.,* **1999,** 32 (4), 837-838, DOI: 10.1107/s0021889899006020.

45. Dolomanov, O. V.; Bourhis, L. J.; Gildea, R. J.; Howard, J. A. K.; Puschmann, H. $OLEX^2$: a complete structure solution, refinement and analysis program, *J. Appl. Crystallog.,* **2009,** 42 (2), 339-341, DOI: 10.1107/s0021889808042726.

# Table of Content Abstract and Graphic

The N,N'-trialkyl-functionalised ureides [(Me$_2$N)C(O)NR] (R = iPr, Cy, tBy Ad, Ph and Mes) act as excellent stabilizing ligands for tin (II) complexes, and the physicochemical properties of these complexes prove their potential as precursors for thin-film deposition. Thermogravimetric analysis has been used to assess the viability of complexes **1-6** as single source precursors for the formation of SnO, with the adamantyl and $^t$butyl derivatives exhibiting clean single-step curves and low residual masses in their TG analyses. The single-crystal X-ray diffraction studies of these derivatives reveal an uncommon $\kappa^2$-N,N' coordination modes.